Eleventh International Conference on Computational Fluid Dynamics (ICCFD11), Maui, Hawaii, USA, July 11-15, 2022

ICCFD11-2022-3802

Machine Learning-Based Physics Inference from High-Fidelity Solutions: Vortical Features & Flow Separation

Nathan Hariharan
HPCMP CREATE™ Technical Operations, Alexandria, VA, 22315

Jennifer N. Abras
HPCMP CREATE™ Quality Assurance Group, Alexandria, VA, 22315

Corresponding author – Nathan Hariharan (nathan.s.hariharan.ctr@mail.mil, nathanaarti@gmail.com)

Abstract: The field of machine learning is broad, covering many different areas and applications. The identification of aerodynamic flow features is one such possible application. Training a machine learning model to classify aerodynamic flow features opens a field of potential applications such as automated data extraction, onboard solution assessment, and volume solution physics comparisons. In this study, Convolutional Neural Network-based ML systems are built to recognize vortical structures and simple flow separation patterns. The system then is deployed to automatically identify & extract such features from 3D flowfields such as rotorcraft wakes. The ML-physics identification system leverages a combination of supervised CNN-learning and non-supervised clustering algorithms. The ML-physics identification methodology is demonstrated for vortex property extraction from high-complex wake physics of hovering rotor blades. A central theme of the ML-inference of physics is the ease and speed with which the automated ML methodology facilitates physics inference from large-scale computed solutions and hence accelerates the process of physics discovery. Potential extensions of the ML-physics inference capability include ML-enabled verification & validation that includes physics comparisons, extraction of high-fidelity physics constructs such as vortical elements and separation patterns to feed to surrogate models, and automated sanity checks to ensure correct end-use of CFD software.

Keywords: Machine Learning, Hi-fidelity Simulations, Physics Inference, Vortices, Flow Separation, CFD, Convolutional Neural Networks

1. Introduction:

Machine learning refers to a vast class of mathematical, statistical, and optimization methods that can infer useful information from observed data [1]. The neural-inspired Deep Learning networks are a compelling class of methods [2][3]. These methods mimic the fundamental canonical elements of human neuron interaction at its core level and have non-linearity inbuilt into the modeling process. In physics-based modeling, deep-learning networks are gaining traction through several avenues, i.e., infusion of physics into the learning mechanism [4], augmenting predictive modeling [5]. A quick literature search yields an exploding list of applications related to aerospace engineering, in general, and aerodynamics, in particular.

A specific form of deep-learning network known as the Convolutional Neural Network (CNN) [6][7] has been spectacularly successful in the field of vision and image processing. In this work, a CNN is architected to classify physics in large-scale 3D fluid-dynamic-simulation result visualization. In present-day workflows involving physics-based simulations, human-in-the-loop visualization of results forms a fundamental basis for inferring physics and assessing the accuracy of the computed results. The primary intent of the current work is to assess if CNN-based deep-learning networks can effectively classify physics such as vortical systems or flow separations in computational simulation results and aid further automation of the workflow for routine simulations.

One of the corollary benefits is to aid verification and validation. Widely used physics-based software tools such as HPCMP CREATE™-AV Kestrel/Helios are subject to rigorous forms of software engineering [8] practices and undergo continuous testing [9] before any new capability is released. With increasing modeling capabilities to simulate real-world model challenges, the permutations required to test the capabilities before a new version is released scale up correspondingly. Traditionally, automated testing of full-up capabilities compares integrated

quantities from "gold-standard" test results and random checks for output quantities to ensure existing capabilities have not been adversely affected. Visual human-engineer spot-checking of underlying field physics is only performed when tests fail. The current effort also explores if visually observable physics (i.e., separation, vortex structure) can be auto-verified by CNN-based systems to ensure high confidence in the automated V&V processes.

An immediate motivation for developing a CNN-based classifier is to extract vortex systems from simulations of rotorcrafts in hover [10]. The flow field underneath a hovering rotor-blade consists of complex 3D vortex dynamics in the wake of the rotor-blade and is non-trivial to capture accurately. A critical aerodynamic efficiency factor for rotorcraft hover performance is the figure-of-merit, a measure of total thrust generated for a given torque required. Understanding the detailed characteristics of the vortical system and how this relates to the predicted hover performance is an essential metric for evaluating a computational model. However, the extraction of such information is a time-consuming, manual process. Furthermore, only a sparse sample of points is feasible when these extractions are performed manually. An automated machine learning-based model to identify vortices can be further developed into an automated system to identify and extract vortex information. By applying this enhanced automated extraction on a routine basis, more insight into the correlation of the wake structure to integrated hover performance results is possible.

2. Machine Learning Methodology and Results:

In this section, the ML methodology to extract vortical information from computed high-fidelity solutions is first discussed. The extraction methodology consists of three broad steps (i) Vortex identification & classification (ii) Vortex center localization, and (iii) Vortex property extraction. In the following section, these steps are described, and sample application results are presented. The final section briefly covers the extension to the method to extract flow separation information.

2.1 ML Vortical Flow Structure Identification

A schematic of the vortex classification Convolutional Neural Net (CNN) is shown in figure 1. The CNN architecture was constructed using TensorFlow 1.15 [11] with the Keras library [12]. The input is processed through a series of convolution and pooling layers before being flattened and then processed through a series of fully-connected layers. The final two-class output provides the prediction confidence of the vortex and no-vortex classes. While the prediction confidence is not a mandatory output for classification, this parameter has proven to be helpful in assessing the quality of the trained CNN. After initial verification with simple canonical structures (figure 2), the method was applied to a high fidelity wake solution from a hovering rotor. While the primary method to generate training data was founded on image processing (figure 2), subsequent improvements eliminated the need for images or image processing in any form and operated on raw floating-point data (figure 3, see Reference [14] for details). Data augmentation for both classification and localization efforts is usually applied to enrich training completeness.

Initial vortex recognition training focused on a simple problem consisting of a single well-formed vortex and a broken-down vortex region of the flow field[14]. Canonical vortical inputs are used to train the CNN and assess its ability to identify a vortex under full and partial conditions consistently. The no-vortex-present samples are used to assess the likelihood of false positives when the vortex is not present. Vertical and horizontal scanning and coarse and fine scan strides are utilized for these tests. Figure 4 shows the demonstration of the CNNs ability to positively identify the presence of a full or partial vortex in a scanning window. The classification CNN stops with the determination of which spatial scanning windows have vortical content present – it makes no attempt to localize the position. Vortex localization is achieved by another CNN and is discussed next.

2.2 ML Vortical Flow Structure Localization

Object localization is closely related to classification. Both employ similar CNN architectures. However, the localization model outputs a set of floating-point numbers between zero and one, representing the vertical and horizontal position of the object in view, instead of a number indicating which class a prediction belongs to. The localization CNN not only provides if there is a vortex in view but also where that vortex center is located. The success of the localization CNN is judged by how close the predicted center is to the actual center, as illustrated in Figure 5. The core center is identified as the location of the peak vorticity magnitude in a vortex.

Figure 6 shows a schematic of the vortex localization CNN. The simple canonical case that has been the focus of the discussion in the prior section is useful for investigating the behavior of the model variations. However, hovering rotor-wakes contain significant variability in vortex dynamics, and the real test of the localization method is the ability to identify vortices and core centers for the full-3D wake geometry. Figure 7 (left) shows volume visualization of the helical vortex structure under a hovering rotor (see Reference [10] for details) – an instance of a computation where the helical vortex structure is largely intact. Figure 7 (right) shows select azimuthal planes in the rotor wake. For clarity, only six sample planes at a resolution of 15 degrees are shown in figure 7 – the scanning process is much finer. These six planes are representative of the general performance of the method on the full wake. The green boxes represent all the locations at which a positive vortex identification was made. Each vortex is positively identified multiple times during the scan process. Each blue point is the associated localization prediction for each positive vortex classification. The classification method was able to target the vortices in view with only a few false positives that an analyst would require additional data to establish if it were a vortex or not. The localization predictions are mostly clustered at the center of the vortices, with a few points located in ambiguous regions.

A more challenging case is the prediction of vortex centers when the computed 3D wake structure exhibits significant wake breakdown (Figure 8 (left), see Reference [10] for details on wake breakdown). A broken-down wake with significant non-helical braid vortex content introduces significantly more ambiguity into the ML prediction process as the wake transitions from coherent helical vortex strands to unstructured vortical flow. The matching ML prediction results are shown in Figure 8. The classification and localization models clearly identify the vortices in view. The predictions taper off in the vertical direction as the tip vortex breaks up.

2.3 ML Vortical Structure Physics Extraction

The overall process of searching for and extracting vortex core data follows multiple stages and is illustrated in the flow chart in Figure 9. The red boxes in this flow chart indicate machine learning-based steps, and the blue boxes indicate non-machine learning-based steps. First, the rotor wake data is loaded into memory. Next, a polar-coordinate-based scan is executed about the rotor axis to search individual azimuthal planes for vortices. Each plane is scanned for vortices within the specified search area using the vortex classification CNN and the localization CNN – as discussed in the last two sections and is labeled under "ML Model Development" Figure 9.

The next step in the vortex physics inference process after vortex classification and vortex-center localization process is the extraction of physics quantities of interest, i.e., core size, circulation etc. This step consists of multiple sub-steps (Figure 9, see Reference [16] for details):

(i) The vortex core center CNN predictions are condensed using an unsupervised ML clustering to identify unique vortex predictions.
(ii) The vortex core physics data is then computed for each of the unique vortex predictions.
(iii) Finally, the resulting point cloud has additional unsupervised ML clustering applied to assign the individual predictions to blades. Once assigned, the wake age is computed for each vortex extraction point.

Figure 10 shows the result of the first step after the application of ML-clustering is completed. The vortex centers are identified uniquely. The core data extraction methods are described in references [15, 16]. The peak vorticity magnitude is identified as the vortex core center. A horizontal slice through the vortex core is used to identify the core radius and peak tangential velocity. Such a process mimics the typical manual method for extracting such information. However, the automated localization and clustering method provides a more accurate estimate of the

vortex center, and hence the process of vortex-property extraction becomes more efficient. Figure 11 shows an example of the processing for a typical helical rotor-wake. In Figure 11, the center image (Region Extraction) illustrates the differences in the core center location. The yellow boxes are the centered extraction regions. The red points are the locations identified as unique vortex-center predictions, and the blue lines are the identified cross-sections across vorticity magnitude peak values. Figure 12 shows the extracted peak-to-peak tangential velocity variations across the vortical structures and illustrates the power of the ML-vortex methodology. The overall vortical content is quite noisy (as seen in Figure 10) with significant 3D braid vortical content, but the ML method is able to track the helical strand well into the third revolution. The method successfully identifies the peak-to-peak profile that represents the core center of each vortex. Extraction of peak-to-peak tip vortex profiles (as a function of wake age) from 3D rotor-wakes is an intensely manual and time-consuming process – the ML-vortex extraction methodology makes it fully automated.

Once the vortex core centers for the four helical strands have been extracted, additional unsupervised clustering is applied to compute the wake age associated with each vortex prediction in the wake. The wake-age computation algorithm is another unsupervised clustering methodology (see reference [16] for details). Figure 13 shows a plot of the final wake vortex center tracking as a function of wake age.

2.4 Example Application of the ML Methodology for Wake Vortex Physics Analysis of Hovering Rotors

In this section, select results from real-world applications for the ML vortex extraction methodology are highlighted. The S-76 rotor-blade hover analysis case is one of the standardized test cases for the AIAA Hover Prediction Workshop [17]. Reference 18 details the underlying hover high-fidelity computations for blade-tip shape variations for the S-76 rotor-blade and variations in operational conditions such as the near-ground effect.

A visual comparison of the ML-predicted trajectories overlaid with the volume visualization solution for an 8° collective anhedral case is shown in Figure 14. The top part of the image is a volume rendering illustrating the portion of the wake scanned by the core extraction process. The bottom part of the image is a comparison of the volume rendering of vorticity magnitude with the core center positions extracted by the ML methodology. This comparison shows that the ML-extracted trajectories are able to track the vortices in the solution. As the effects of the numerical wake breakdown strengthen with wake age, the tip vortices begin to break up, and the core profiles deviate farther and farther from the axisymmetric ideal profile before disappearing. As expected, the ML-based predictions also become more broken up as a function of wake age in line with the volume data. In addition, the vortex-centers of the individual blades are not identical as expected. Figure 14 (right) also compares the radial position of helical strands with wake age. Even though the overall system is axi-symmetric, vortical interactional dynamics introduce small amounts of asymmetry at the individual helical strand level.

Figure 15 provides a verification of the ML-extraction for a quasi-steady S-76 hover computation where there is no wake breakdown. Figure 15 compares the ML-extracted vortex position (radial, vertical) and core size against manually extracted values - the results are indistinguishable. Whereas the manual extract is done only at select azimuthal locations for a single blade and takes about a day of painstaking work, the ML-extraction takes is automated and takes around ten minutes. The ML method can also extract much finer-scale wake age data for multiple blades for individual-blade comparison than is possible with manual extraction.

One of the key performance parameters for a hovering helicopter is the rotor blade's aerodynamic efficiency – known as the figure of merit (FM) [18]. FM is a measure of the ratio of the thrust generated by a rotor for a given engine torque at operating conditions. Rotor-blade designers often focus on the tip shape of the rotor as a mechanism to boost FM. Figure 16 shows typical blade-tip variations studied for the S-76 rotor-blade. Incorporating a tip-anhedral or sweep is often employed to alter the tip loading and strength/position characteristics of the generated tip vortex. Comparing the ensuing tip-vortex trajectory is of keen interest to figure out the physics driving FM changes due to tip-shape changes. Figure 17 shows the ML-extracted tip vortex trajectory/circulation/core-size comparisons. Figure 18 shows similar physics extractions for typical variations in rotor operational states for a given tip shape, i.e., operating near the ground vs. away from the ground. Detailed discussions on the implications of the differences in vortex trajectory/positions are beyond the scope of this paper (see Reference 18). However, the central theme illustrated from the above two use-cases is the ease and speed with which the automated ML-vortex methodology facilitates physics inference from large-scale computed solutions and hence accelerates the process of physics discovery.

2.5 ML-Classification for Separated Flows: Preliminary Analysis

The ML methodology described in this paper has broader applications to target other physics features such as flow separation or shocks. Specifically, the automated identification of flow separation has many practical applications, including verification of engineering evaluations for sanity checks. Reference 19 shows initial forays into extending the ML methodology to flow separation. The preliminary image-based version of the CNN in Figure 1 was modified to train using 2D flow separation over a NACA0015 airfoil. Figure 20 shows the CNN (from Reference 19) and sample training images. It is easy to distinguish the differences between images with an AoA of 0° vs. 22°. However, the ML methods' success will depend on whether it can pick up the transition to stall accurately as the AoA goes through 12-13 degrees for the NACA0015. The CNN was trained with images with AoA's from 0° to 8° (fully attached flows) and 14° to 22 (fully separated flows). After training and verifying with 2D image sets, the methodology was applied to a 3D twisted NACA wing, as shown in figure 21. Spanwise scanning is done to predict the spanwise station where the stall first occurs. Figure 22 (from Reference 19) compares the stall-point prediction accuracy when different image sets are used for the training and prediction. Further work is required to automate primitive-variable based truly 3D flow separations.

3. Conclusions and Future Work:

A machine learning framework has been developed to automatically extract flow features such as vortices and flow separations from large 3D computational data sets. The machine learning models discussed in this effort are a significant advancement over the previously published efforts. While the primary method to generate training data was founded on image processing, subsequent improvements eliminated the need for images or image processing in any form and operated on raw floating-point data directly obtainable from high-fidelity simulations. The methodology has been refined specifically for extracting tip vortex structures for rotors in hover. The ML-vortex identification system leverages a combination of supervised CNN-learning and non-supervised clustering algorithms. Illustrative results from automated extraction of wake vortex physics for AIAA Hover Prediction Workshop S-76 rotor blade hover solution were highlighted. Preliminary results from an investigation of the identification of separated flows over 3D wings were also presented. Whereas the manual extract process takes about a day of painstaking work, the ML extraction is automated and takes around ten minutes. The ML method can also extract much finer-scale spatial/temporal wake vortex data without human intervention. A central theme of the ML-inference of physics is the ease and speed with which the automated ML-vortex methodology facilitates physics inference from large-scale computed solutions and hence accelerates the process of physics discovery.

The method promises to automate & enormously speed up the human-in-the-loop aspect of visualization and extraction of physics inference from 3D high-fidelity CFD simulations. Such a capability will also enable ML-enabled verification & validation that includes physics comparisons, extraction of high-fidelity physics constructs such as vortical elements and separation patterns to feed to surrogate models, and automated sanity checks to ensure correct end-use of CFD software. Current training methods for the classification and localization CNNs rely on 2D slices from 3D data. Future work will target direct three-dimensional training. Using three-dimensional data will allow the generalization of vortex structure extraction and accommodate broader use-cases such as high Angle-of-Attack aircraft aerodynamics.

Acknowledgments

Material presented in this paper is a product of the CREATE (Computational Research and Engineering for Acquisition Tools and Environments) element of the U.S. Department of Defense HPC Modernization Program. In addition, the authors would like to acknowledge the support of the supercomputing resources provided by the HPCMP, in particular, the Air Force Research Lab (AFRL) and the Army Engineer Research and Development Center (ERDC). The blade and hub models, test reports, and standardization guidance provided through the AIAA Hover Prediction workshop (HPW) are also gratefully acknowledged.

REFERENCES

1. Hastie, T., Tibshirani, R., and Friedman, J., "The Elements of Statistical Learning: Data Mining, Inference and Prediction," Springer-Verlag, New York, 2009.
2. Goodfellow, I., Bengio, Y., and Courville, A., "Deep Learning," MIT Press, 2016.
3. Ng, A., "Deep-Learning," deeplearning.ai, 2018.
4. Raissi, M., Perdikaris, P., and Karniadakis, G., "Physics-informed Neural Networks: A deep-learning framework for solving forward and inverse problems involving nonlinear partial differential equations," Journal of Computational Physics, Volume 378, pp 686-707, February 2019.
5. Singh, A., Medida, S., Duraisamy, K., "Machine Learning-augmented Predictive Modeling of Turbulent Separated Flows over Airfoils," AIAA Journal, Volume 55, Number 7, July 2017.
6. LeCun, Y., Bottou, L., Bengio, Y., and Haffner, P., "Gradient based learning applied to document recognition," Proceedings of the IEEE, Volume 86, Issue 11, November 1998.
7. LeCun, Y., Kavukcuoglu, K., and Farabet, C., "Convolutional networks and applications in vision," IEEE International Symposium on Circuits and Systems, Paris, France, May/June 2010.
8. Hallissy B., Hariharan N., Laiosa J., Shafer T., Hine D., Forsythe J., Abras J., Lillian C., and Dahl C., "CREATE-AV quality assurance: best practices for validating and supporting computation-based engineering software," 52nd AIAA Aerospace Sciences Meeting, National Harbor, MD, January 13-17, 2014.
9. Kendall, R., Hariharan, N., and Park, L., "HPCMP CREATETM Operational Practices Guide," HPCMP CREATETM White Paper, January 2020.
10. Hariharan, N., Abras, J., and Narducci, R., "An Overview of Wake Breakdown in High-Fidelity Simulations of Rotor-in-Hover," Vertical Flight Society 76th Annual Forum, Virginia Beach, VA, October 6-8, 2020.
11. Abadi, M., Agarwal, A., Barham, P., Brevdo, E., Chen, Z., Citro, C., Corrado, G., Davis, A., Dean, J., Devin, M., Ghemawat, S., Goodfellow, I., Harp, A., Irving, G., Isard, M., Jozefowicz, R., Jia, Y., Kaiser, L., Kudlur, M., Levenberg, J., Mané, D., Schuster, M., Monga, R., Moore, S., Murray, D., Olah, C., Shlens, J., Steiner, B., Sutskever, I., Talwar, K., Tucker, P., Vanhoucke, V., Vasudevan, V., Viégas, F., Vinyals, O., Warden, P., Wattenberg, M., Wicke, M., Yu, Y., and Zheng, X., "TensorFlow: Large-scale machine learning on heterogeneous systems," https://www.tensorflow.org/, 2015.
12. Chollet, F., et al., "Keras," https://keras.io, 2015.
13. Ahrens, J., Geveci, B., Law, C., "ParaView: An End-User Tool for Large Data Visualization, Visualization Handbook," Elsevier, 2005, ISBN-13: 978-0123875822
14. Abras J., Hariharan N., "Application of Machine Learning to Automate Flow Physics Identification in Computed Solutions: Hover Rotor Wake Vortex Identification and Breakdown Analysis," 59th AIAA Aerospace Sciences Meeting, Nashville, TN, January 11-15, 2021.
15. Abras, J., and Hariharan, N., "Machine Learning Based Physics Inference from High-Fidelity Solutions: Vortex Classification and Localization," 60th AIAA Aerospace Sciences Meeting, San Diego, CA, January 3-7, 2022.
16. Abras, J., and Hariharan, N., "Machine Learning Based Physics Inference from High-Fidelity Solutions: Vortex Core Extraction," 60th AIAA Aerospace Sciences Meeting, San Diego, CA, January 3-7, 2022.
17. AIAA Hover Prediction Workshop (HPW), AIAA HPW | Hover Prediction Workshop | Rotorcraft Hover (aiaa-hpw.org)
18. Abras, J., and Hariharan, N., "Automated Inference of Vortex Core Physics of Hovering Rotor Wakes Using Machine Learning Techniques," Vertical Flight Society's 78th Annual Forum & Display, Ft. Worth, TX, May 2022.
19. Nathan, R., "Application of Machine Learning to Automate Flow Separation Identification in Computed Solutions," 60th AIAA Aerospace Sciences Meeting, San Diego, CA, January 3-7, 2022.

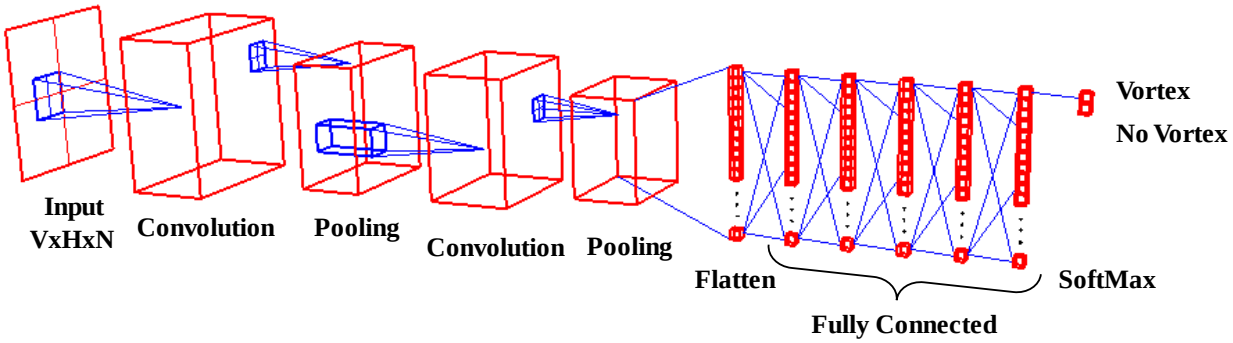

Figure 1. Convolutional Neural Net Architecture to classify if vortex is present in the scanning domain [14].

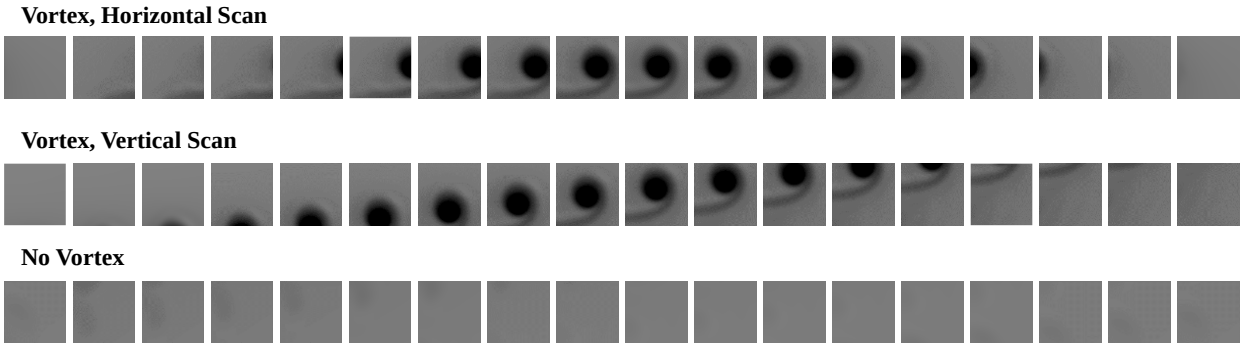

Figure 2. Sample training images for simple demonstration problem [14].

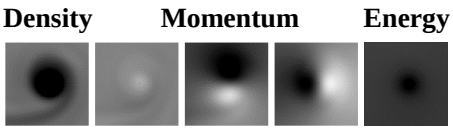

Figure 3. CFD primate variable inputs to train for vortex classification [14].

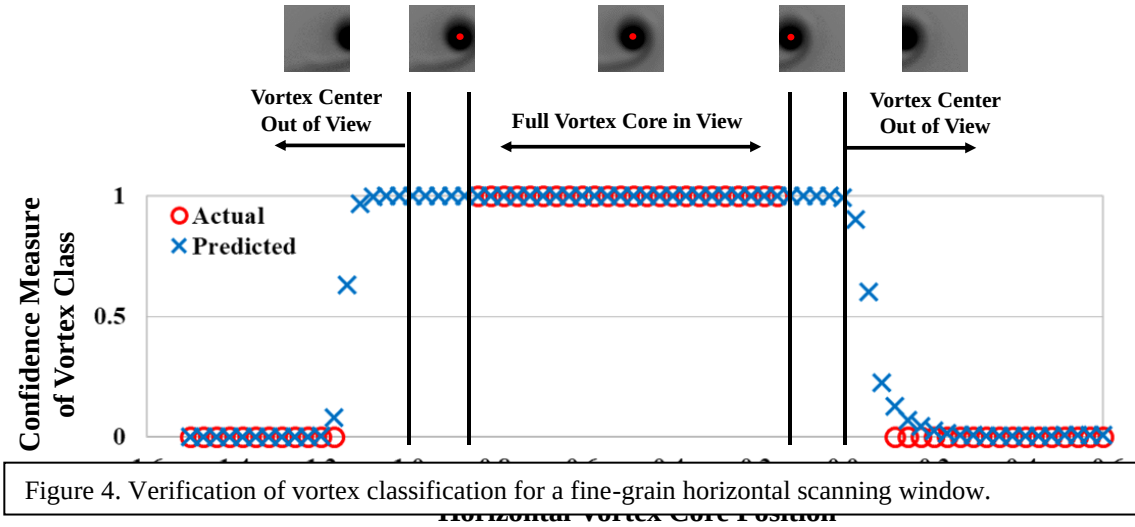

Figure 4. Verification of vortex classification for a fine-grain horizontal scanning window.

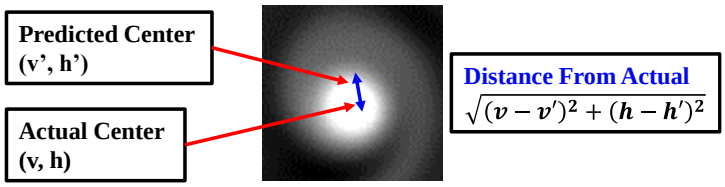

Figure 5. Vortex localization training metric.

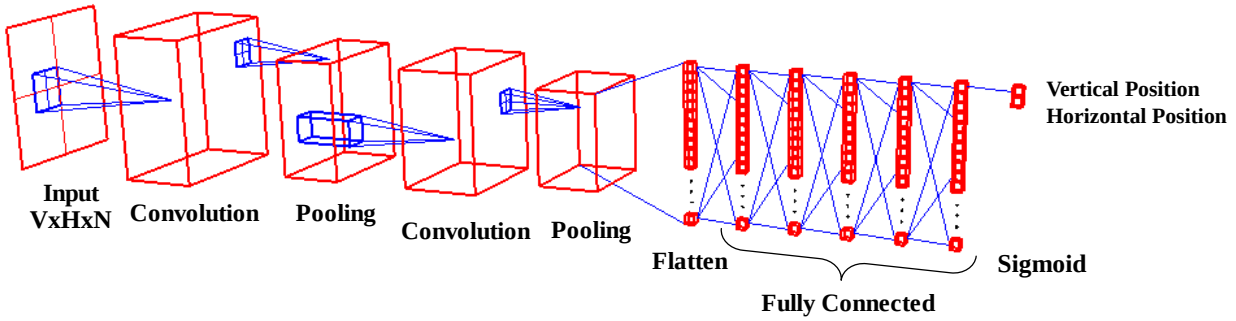

Figure 6. Vortex localization CNN.

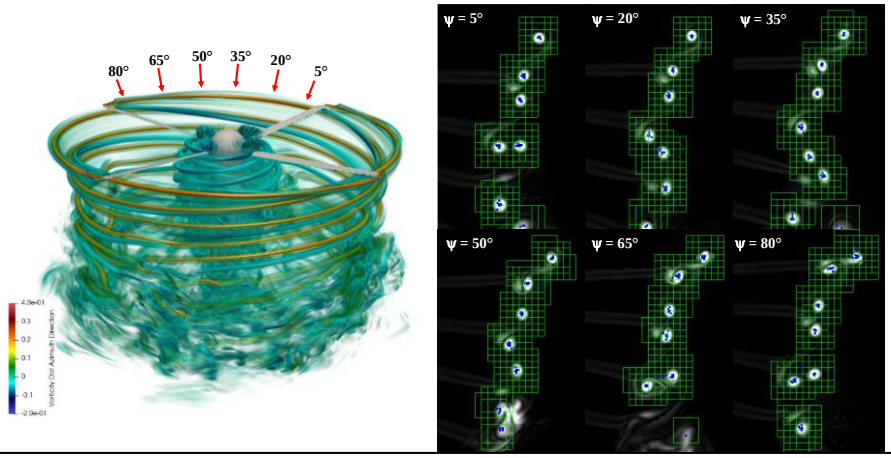

Figure 7. Raw classification (green boxes) and localization (blue points) predictions on a typical rotor wake [15].

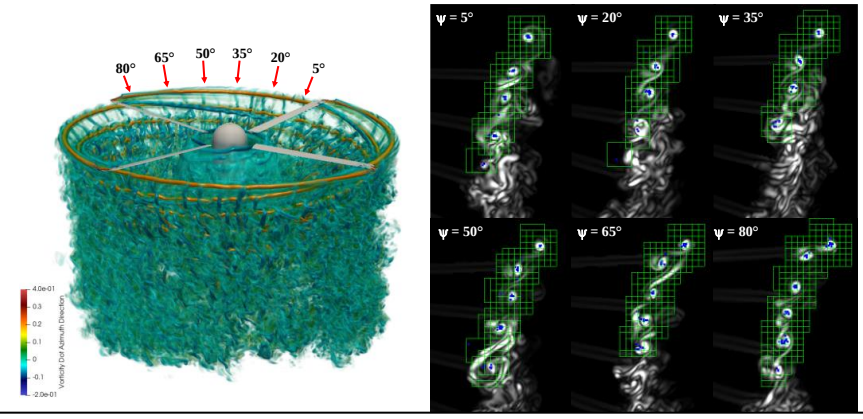

Figure 8. Classification & Localization with broken down wake structure[15].

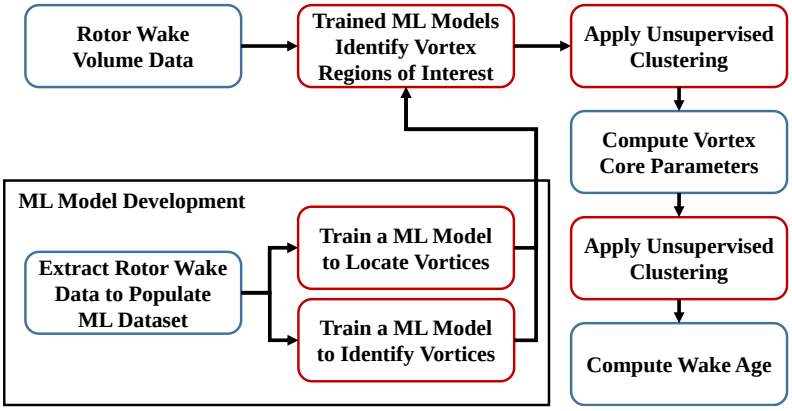

Figure 9. Overview of the classification/localization/extraction process [16].

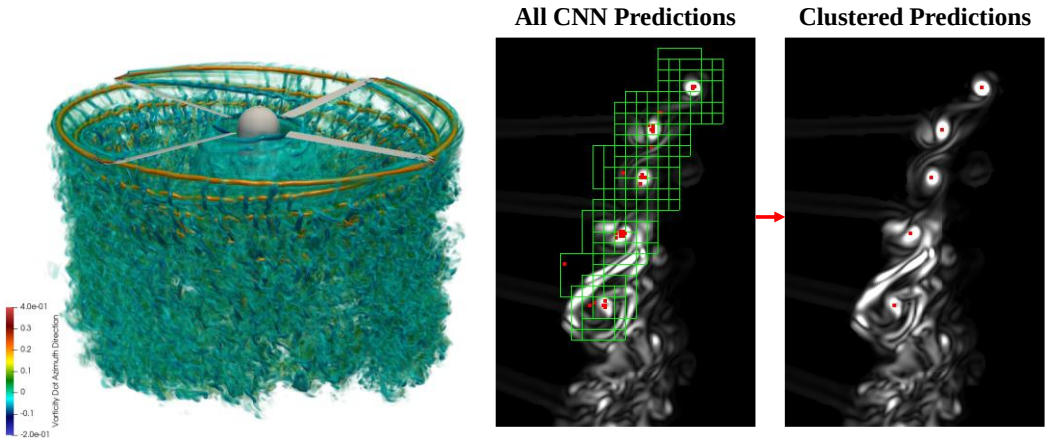

Figure 10. ML clustering eliminates outliers from ML-classification (broken down wake) [16].

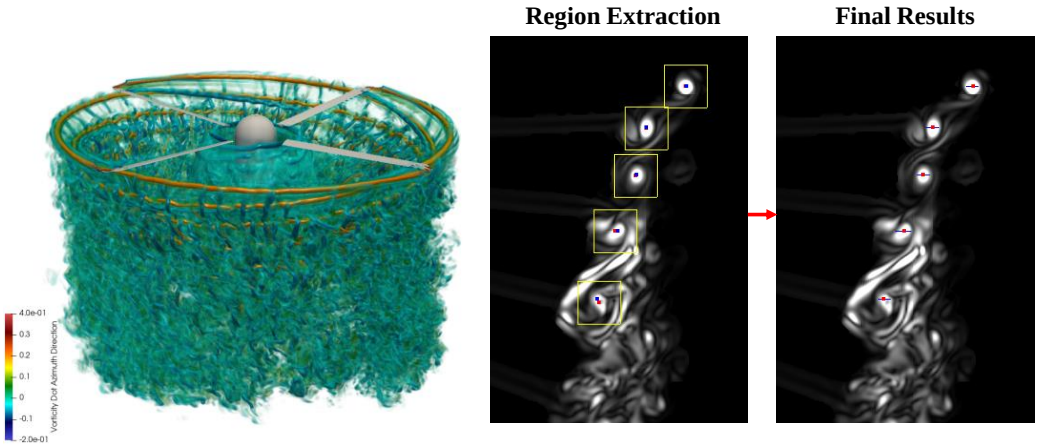

Figure 11. Vortex region extraction and extraction of core profile properties [16].

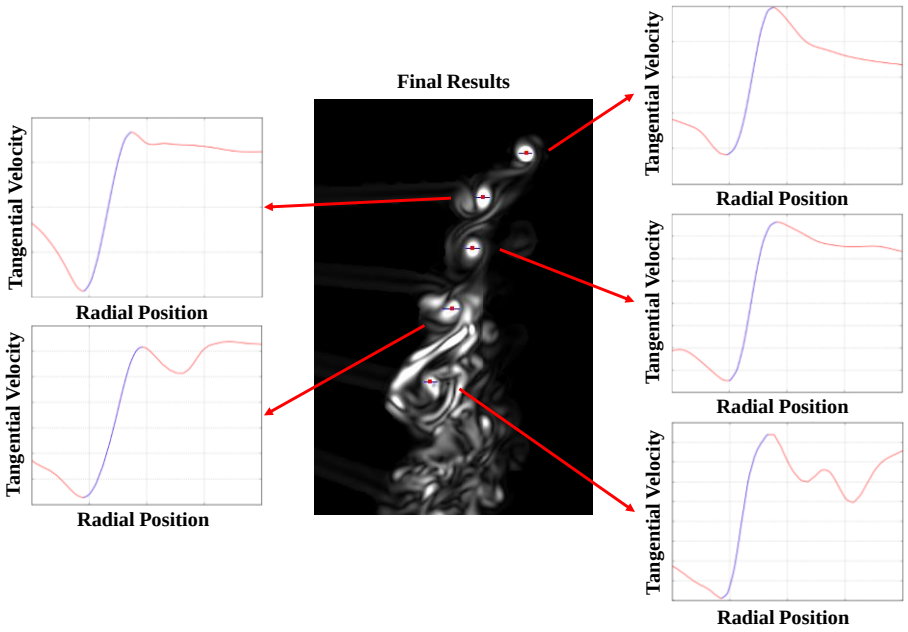

Figure 12. Peak to peak tangential velocity extraction [16].

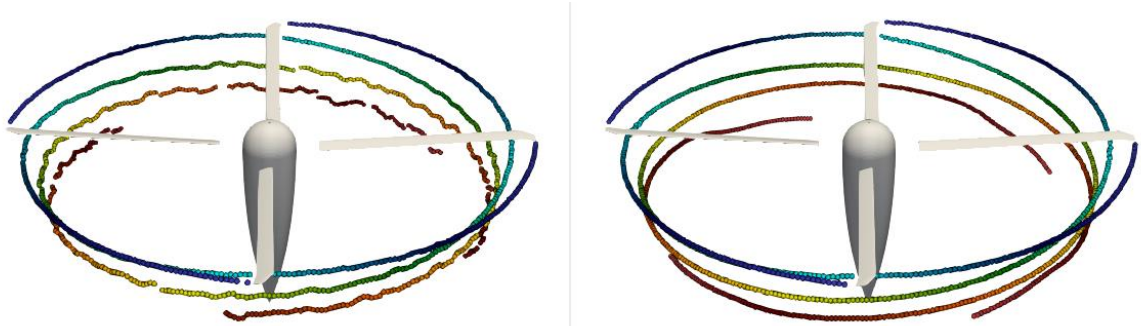

Figure 13. Wake age extraction for broken down wake (left) and preserved wake (right) [16].

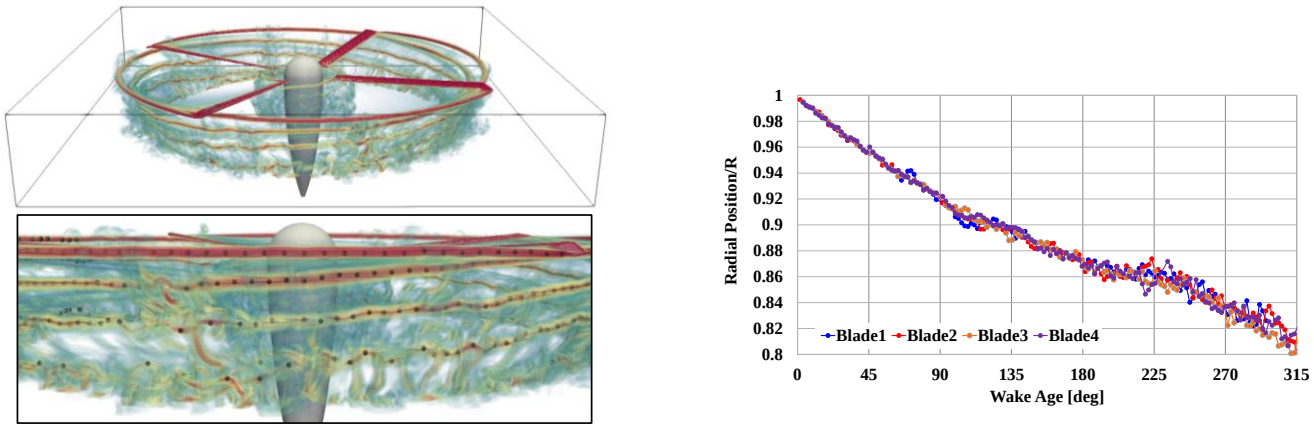

Figure 14. VoREX extraction of core centers for S-76 planform (Left) Overlaid with wake volume viz, (Right) Radial location of the vortex center for the four blades [17]

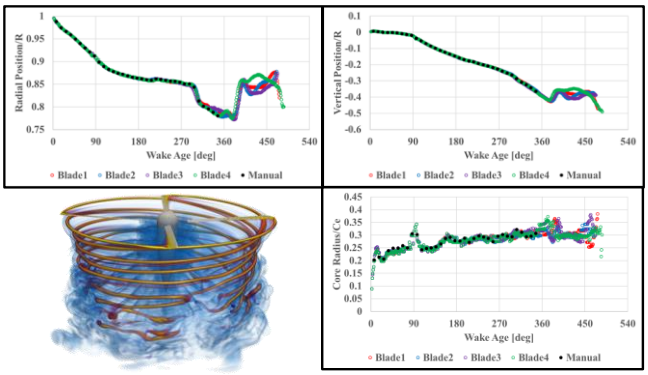

Figure 15. Verification of ML-extracted wake positioning vs. manual process for the S-76 rotor [17]

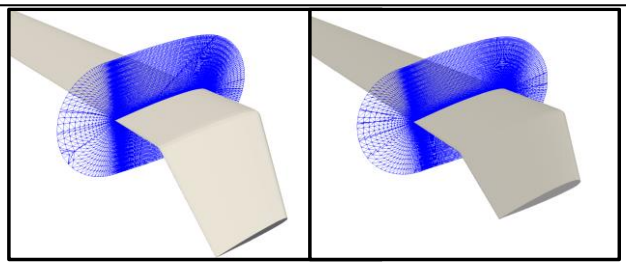

Figure 16. Blade tip variations for the S-76 rotor [17]

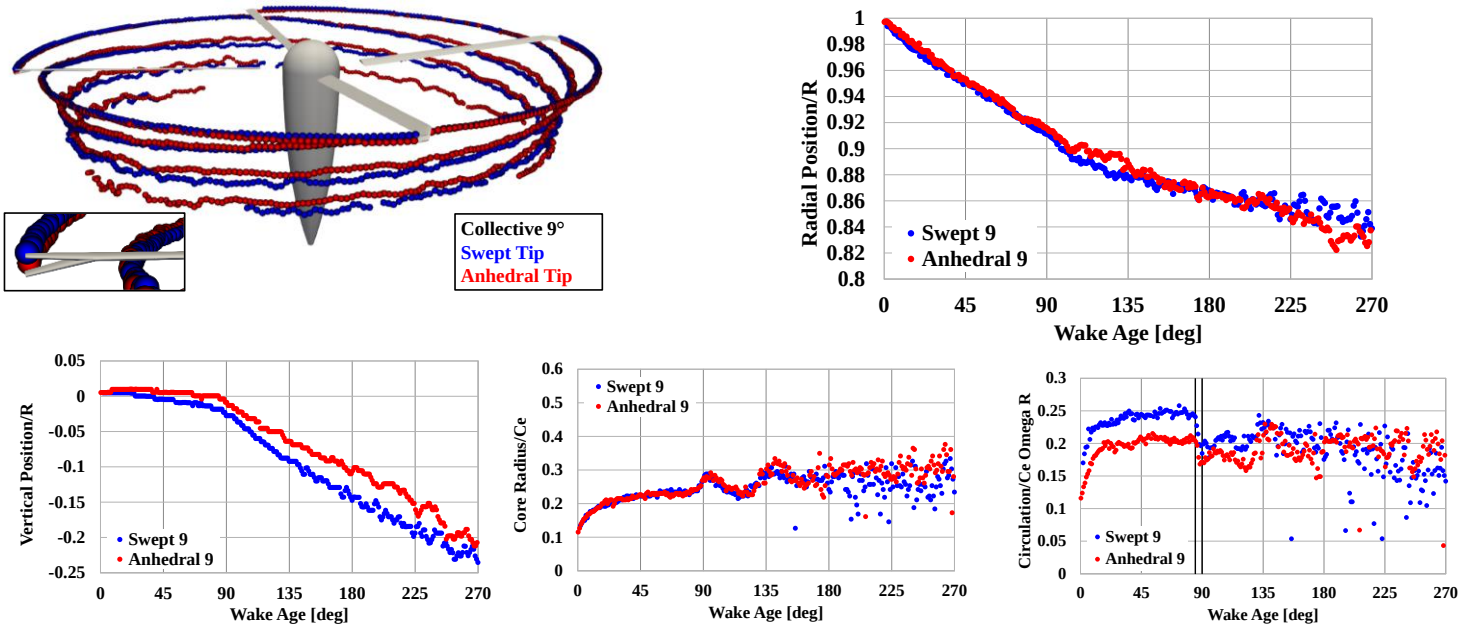

Figure 17. Wake vortex physics comparison for the S-76 rotor tip-shape variations [17]

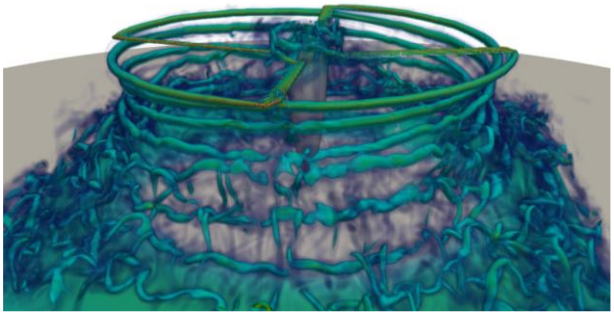

Figure 18. Hovering rotor in ground effect (IGE)

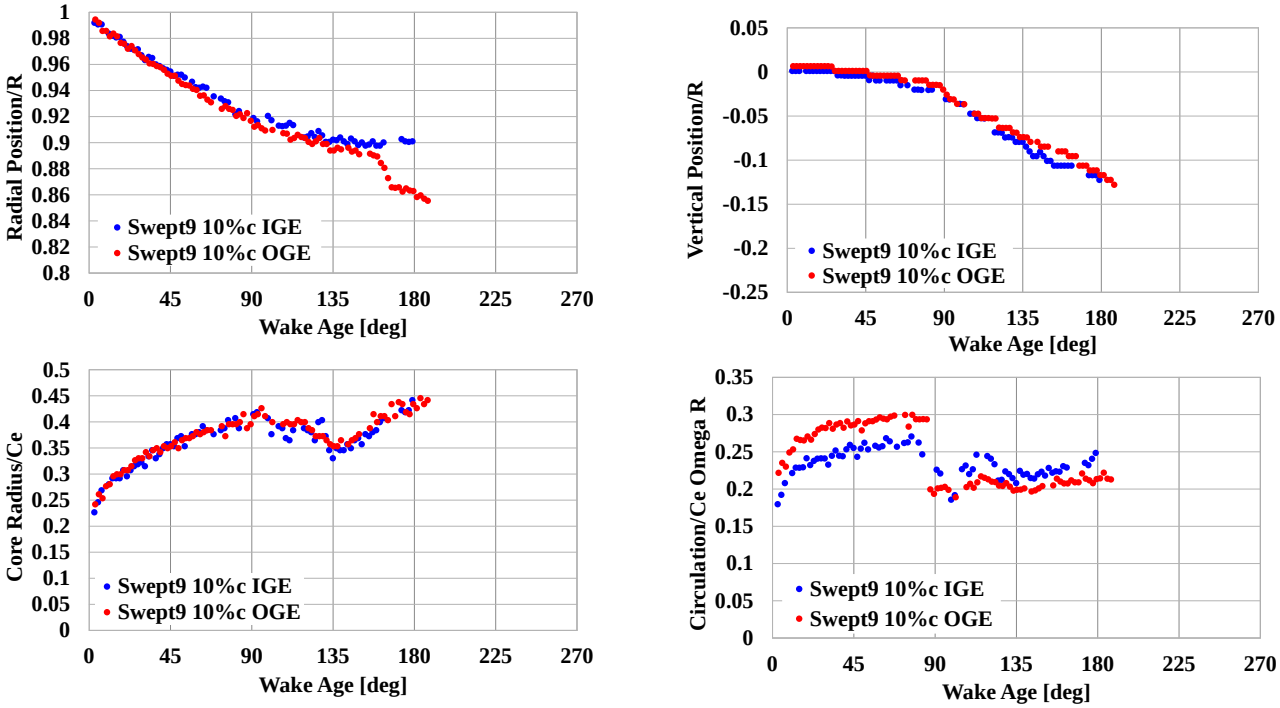

Figure 19. Wake vortex physics comparison for the S-76 rotor in ground effect (IGE) vs. out-of-ground effect (OGE).

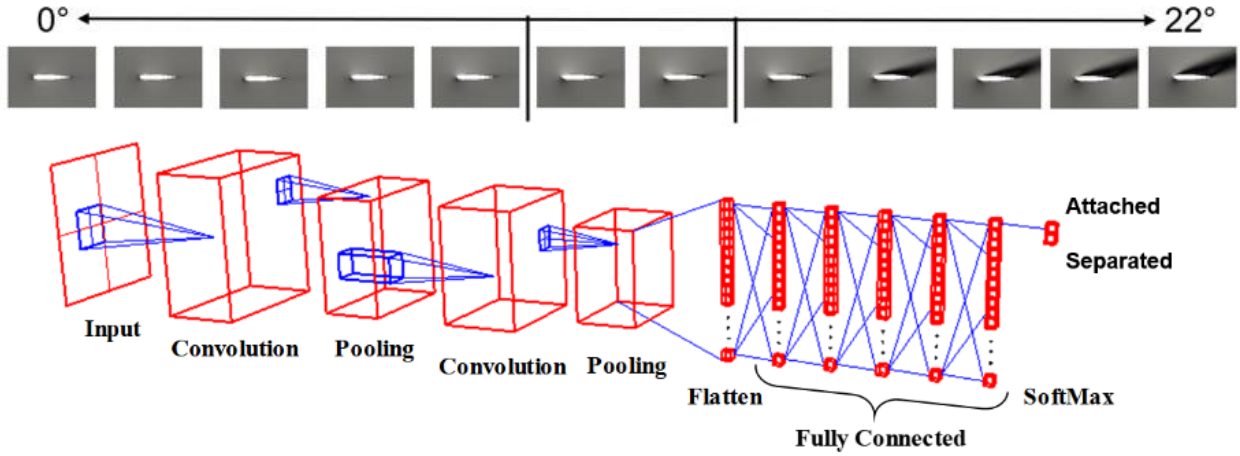

Figure 20. CNN and image training set for exploratory study on identifying separated flows [19].

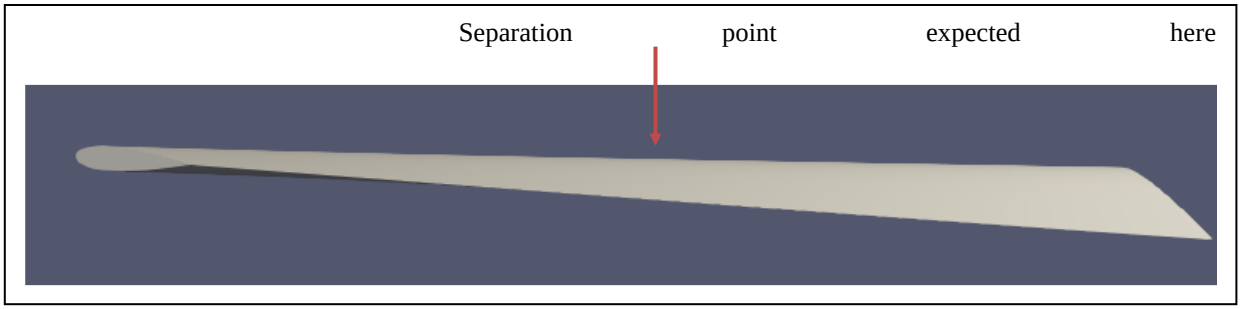

Figure 21. Linearly twisted NACA0015 wing planform (0-30 degrees).

50x50	Density	Momentum	Vortmag	Energy
Accuracy	0.95	0.94	0.94	0.89
Time	13:00	12:22	12:22	13:03
Point of Separation	10 °	13 °	14 °	10 °
Error	3 °	0 °	1 °	3 °

Figure 22. CNN prediction of point of separation and error for different training scalar sets.